On LiDAR-assisted wind turbine retrofit control and fatigue load reductions

Lio, Wai Hou; Meng, Fanzhong; Larsen, Gunner Chr.

Published in:
Turbine Technology; Artificial Intelligence, Control and Monitoring

Link to article, DOI:
10.1088/1742-6596/2265/3/032072

Publication date:
2022

Document Version
Publisher's PDF, also known as Version of record

On LiDAR-assisted wind turbine retrofit control and fatigue load reductions

On LiDAR-assisted wind turbine retrofit control and fatigue load reductions

Wai Hou Lio, Fanzhong Meng and Gunner Chr. Larsen

Department of Wind Energy, Technical University of Denmark (DTU), DK-4000 Roskilde, Denmark

E-mail: wali@dtu.dk

Abstract. The use of upstream wind speed measurement has motivated the development of LiDAR-assisted control for enhancing rotor speed tracking and fatigue structural load reductions. However, conventional LiDAR-assisted control designs often require altering the existing controller architecture, for example, by sending an additional feed-forward pitch angle signal to the pitch actuator or by incorporating the feed-forward pitch rate into the feedback controller. This work proposes LiDAR-assisted retrofit control solutions that can be implemented without any prior knowledge or modifications of the existing feedback controller. Specifically, the feed-forward pitch action is provoked by modifying the rotor speed measurement. Three retrofit methods are proposed according to the level of retrofit requirement and complexity. Numerical simulation results showed that all three LiDAR-assisted retrofit solutions could achieve good thrust-related load reductions. Thus, the proposed LiDAR-assisted retrofit solutions present a simple control upgrade to extend the lifetime of existing turbines.

1. Introduction

Fatigue load reduction is one of the key objectives of wind turbine control design. Conventional wind turbine controllers are typically developed based upon a feedback mechanism. The control actions based on the feedback measurement respond to wind disturbances/events that have already taken place on the turbine structure, thus leading to the inevitable higher fatigue damage on the key turbine components as well as higher actuator effects to counteract the wind disturbance. Recent development in remote sensing technology, such as light detection and ranging (LiDAR) systems, enables the turbine to possess accurate measurements of the incoming wind at some upstream distance from the wind turbine in focus. Based on this incoming wind information, the turbine controller can plan its control actions well ahead before the wind disturbance hits the turbine structure, thus, resulting in reductions in turbine fatigue loads. Therefore, the availability of reliable LiDAR systems has motivated the study of feed-forward/LiDAR-assisted control of wind turbines.

LiDAR-assisted wind turbine control has been a popular topic over the past two decades. Harris el at. [1] conducted one of the earliest studies of feed-forward control. Later, an increasing number of studies employed LiDAR systems to assist the collective pitch control approach for improving rotor speed regulation and reducing fatigue load. (See [2]). In addition, some studies (e.g. [3]) used LiDAR systems to improve individual pitch control for reducing loads on the blades as well as on other turbine structures. The work presented in e.g. [4] demonstrated that the wind measurements could naturally be incorporated into a model predictive control (MPC)

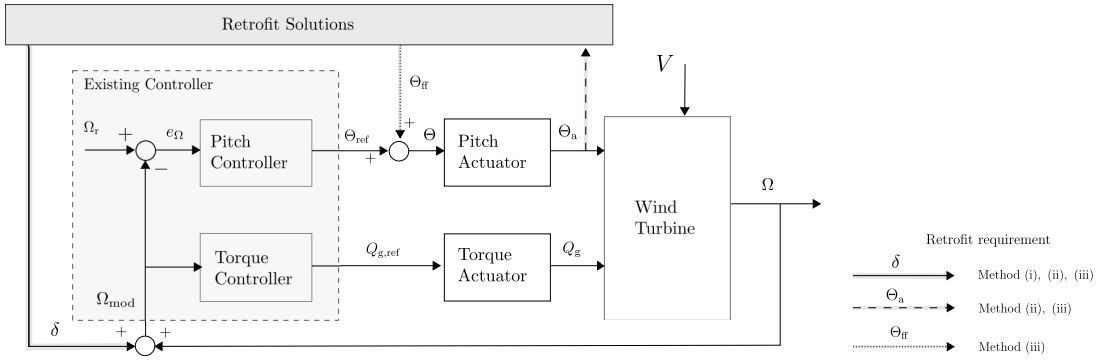

Figure 1: The proposed three retrofit solutions. (1) The retrofit controller modifies the rotor speed measurement Ω by adding a retrofit signal δ. (2) In addition to rotor speed modification, the retrofit controller can measure the actuator pitch angle Θ_a. (3) The retrofit controller changes not only the rotor speed measurement, but also the pitch angle reference signal by adding an additional signal Θ_{ff}.

formulation, thus leading to an improvement in load alleviation. Furthermore, many full-scale tests, e.g. [5], have been conducted for demonstrating the efficacy of LiDAR-assisted control. More recently, an IEA Wind task was set up to support the adoption of LiDAR technology for wind energy applications [6, 7].

Nonetheless, a common assumption in the literature is that the control architecture in a wind turbine can be easily modified. However, changing the controllers in turbines is often costly and time-consuming, for example, the certification process of turbines may need revision. Some studies have proposed methods to retrofit or add-on another layer of control upon existing control architecture. For example, the study by [8] fitted a rotor speed over-speeding protection controller upon the existing controller. Another study [9] proposed an add-on algorithm to ensure the turbine loads within the design load envelope. In addition, the studies by [10, 11] incorporated a LiDAR-assisted MPC controller upon an existing controller, where the input from the additional controller is optimized based upon the incoming wind measurements and constraint information. However, these approaches require modification of the pitch actuator, which might be complicated and expensive.

This work proposes the LiDAR-assisted control retrofit solutions that require no prior knowledge of the existing feedback controller. The feed-forward pitch action is provoked by modifying the rotor speed measurement signal. As shown in Figure 1, three retrofit methods were proposed based on the level of retrofit requirement:

(i) Method 1: the retrofit controller only modifies the rotor speed measurement;

(ii) Method 2: the retrofit controller modifies the rotor speed with the measurement of the current pitch angle from the pitch actuator;

(iii) Method 3: the retrofit controller changes not only the rotor speed measurement, but also the pitch angle demand to the pitch actuator. This case serves as a benchmark, as it is closer to the conventional approach.

The key benefit of these retrofit solutions from the industrial perspective is, that they can be easily implemented on an existing turbine without any modification of the embedded controller. Thus, this simple control upgrade can extend the lifetime of many existing turbines.

The remainder of the paper is structured as follows. In Section 2, the background of the traditional LiDAR-assisted control is presented. Section 3 presents the design of three proposed retrofit methods. In Section 4, the proposed methods are validated using simulations results and

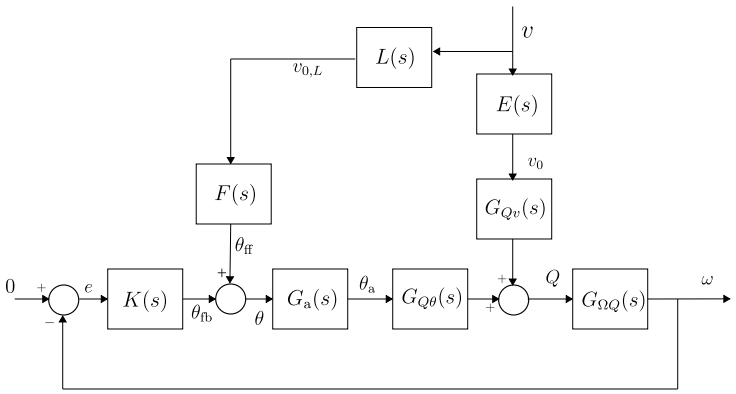

Figure 2: Block diagram of a linear model of tradition LiDAR-assisted feed-forward control.

lifetime structural fatigue loads are evaluated. This is then followed by conclusions and future works in Section 5.

2. Background

A typical LiDAR-assisted control block diagram is depicted in Figure 2 (See [5]). Notice the notations used in Figure 2 represent the deviations, as the turbine linear model is linearised around an operating point in above-rated wind speed, typically at rated wind speed $V = v_{\text{r}}$, rated rotor speed $\Omega = \Omega_{\text{r}}$ and optimal pitch angle $\Theta = 0$ (See [12]). The feedback controller $K \in \mathcal{R}$[1] is designed to regulate the rotor speed deviation $\omega := \Omega_{\text{r}} - \Omega$ by adjusting the collective pitch angle command θ_{fb}. The actuator dynamics is denoted as $G_{\text{a}} \in \mathcal{R}$. The transfer functions mapping the actuator pitch angle θ_{a} and wind speed v_0 to the aerodynamic torque Q are represented by $G_{Q\theta}, G_{Qv_0} \in \mathcal{R}$ respectively, whilst the drive-train dynamics mapping the torque to rotor speed is denoted as $G_{\Omega Q} \in \mathcal{R}$. The wind field v in front of the turbine evolves to v_0 via an evolution $E \in \mathcal{R}$, and the measurement in front of the turbine by the LiDAR system $L \in \mathcal{R}$ is denoted as $v_{0,L}$. The wind disturbance can be perfectly compensated if the feed-forward pitch command θ_{ff} is designed as follows:

$$v_0 = EL^{-1} v_{0,L}, \tag{1}$$

$$\theta_{\text{ff}} = -\left(G_{\Omega Q} G_{Q\theta} G_{\text{a}}\right)^{-1} G_{\Omega Q} G_{Qv} v_0, \tag{2}$$

The LiDAR-assisted control design is typically decoupled into two problems: (i) how to map the LiDAR measurement $v_{0,L}$ into the rotor effective wind speed v_0; (ii) how to translate the wind speed v_0 into a good feed-forward pitch action θ_{ff}.

To solve the first problem, the transfer function $G_{\text{EL}} := EL^{-1} \in \mathcal{R}$ in Eq (1) mapping $v_{0,L}$ to v_0 needs to be identified. A simplification is often made due to the complexity of the evolution and the LiDAR spatial averaging dynamics. Due to the low pass effect of the LiDAR, the transfer function is typically modelled as an adaptive first-order Butterworth filter with some delays, defined as follows:

$$G_{\text{EL}} = \frac{1}{\tau_{\text{c}} s + 1} e^{T_{\text{d}} s}, \tag{3}$$

where $\tau_{\text{c}} := 1/(2\pi f_{\text{c}})$ is the time-constant of the filter, and its cut-off frequency $f_{\text{c}} := k_{0.5}\bar{U}/(2\pi)$ is computed based on the coherence bandwidth $k_{0.5}$, where the magnitude-square coherence

[1] let $\mathcal{R}$ denote the set of real rational transfer functions.

$\gamma^2 = 0.5$. The mean wind speed is denoted as $\bar{U}$. The time delay T_d is defined as follows:

$$T_\mathrm{d} = \frac{D}{\bar{U}} - T_\mathrm{filter} - \tau. \tag{4}$$

The first term assumes the wind flow obeys Taylor's frozen turbulence hypothesis, where the turbulent structures move as frozen entities transported by a characteristic mean wind speed $\bar{U}$ over the measured distance D. The hypothesis is proven valid up to a certain frequency range as validated in an experiment [13]. The time delay introduced by the low-pass filter is approximated by T_filter. The time τ represents modelling errors, for example, the effect of the rotor induction zone.

Now, to solve the second problem, the system transfer functions in Eq (2) need to be modelled. Typically, the drive-train and actuator dynamics ($G_{\Omega Q}$ and G_a) are modelled as first-order low-pass systems, whilst the aerodynamic torque mappings G_{Qv} and $G_{Q\theta}$ are approximated by aerodynamic sensitivities $\partial Q/\partial v, \partial Q/\partial \theta \in \mathbb{R}$, respectively. Thus, the transfer function in Eq (2) is typically a non-causal system. Thus, a common practice to calculate the feed-forward pitch angle is simply based on the steady-state pitch curve with some preview time T, defined as follows:

$$\theta_\mathrm{ff}(t) = \theta_\mathrm{ss}\left(v_0(t+T)\right). \tag{5}$$

Instead of adding the feed-forward pitch angle directly into the pitch command, pitch rate $\dot{\theta}_\mathrm{FF}$ of Eq (5) is typically used for practical reasons (e.g. [14,15]). In particular, the feed-forward pitch rate is often added to the input of the feedback integrator. The reason is that since the feed-forward pitch angle takes over some low-frequency speed regulation duty, that renders the feedback control action handles the high-frequency load alleviation, operating around zero. Thus, adding the feed-forward pitch rate into the feedback integrator can prevent saturating the feedback action by the lower pitch limits.

An alternative feed-forward control design is to move the current pitch angle gradually to the target steady-state angle that corresponds to the preview wind speed over the preview period [16,17]. The pitch rate demand is defined as follows:

$$\dot{\theta}_\mathrm{FF}(t) = \frac{\theta_\mathrm{ss}\left(v_0(t+T)\right) - \theta(t)}{T}. \tag{6}$$

Notice that both approaches in Eqs (5) and (6) are similar. In Eq (5), the preview time considers the actuator dynamics and time-delay caused by the rotor dynamics, whilst in Eq (6), the preview time is typically much longer and take into account the current pitch angle. In addition, in Eq (5), the feedback and feed-forward design is strictly separated based on the concept of 'two degrees of freedom', where the feed-forward design does not influence the closed-loop robustness properties. Nonetheless, most of the LiDAR-assisted control design is conducted in a 'retrofit' sense [18], where the feed-forward controller is designed at a later stage than the feedback controller. The gain of the feedback controller is often needed to be re-tuned anyways for optimising the performance. Thus, one might question the importance of obeying the concept of 'two degrees of freedom'. This topic is beyond the scope of this work.

3. Methodology

The majority of these LiDAR-assisted control methods assumed either the pitch rate (or angle) can be added to the feedback integrator or to the pitch actuator, or the feedback controller gain can be adjusted arbitrarily. By limiting these options, this study investigates three LiDAR-assisted wind turbine retrofit control strategies, as depicted in Figure 1, and these three strategies are ordered in terms of the level of retrofit complexity.

3.1. Method 1: modifying the rotor speed measurement solely

In this approach, the retrofit controller modifies the rotor speed measurement solely by adding a retrofit signal δ to the measurement. This method provokes the change of controller action simply by modifying the measurement of the rotor speed whilst maintaining the existing controller structure unchanged. This is the simplest/cheapest retrofit solution.

Compared to the traditional feed-forward approaches in Section 2, the design task in Method 1 is to map the LiDAR measurement v_0 to the retrofit fit signal δ. To begin, in Figure 2, the pitch angle command to the pitch actuator is defined as follows:

$$\begin{aligned} \theta &= \theta_{\text{fb}} + \theta_{\text{ff}}, \\ &= K\omega + \theta_{\text{ff}}. \end{aligned} \tag{7}$$

The pitch actuator command in Method 1 is expressed as follows:

$$\theta = K(\omega - \delta). \tag{8}$$

Combining Eq (7) and (8) yields:

$$\begin{aligned} &K\omega + \theta_{\text{ff}} = K(\omega - \delta) \quad \Rightarrow \\ &\delta = -K^{-1}\theta_{\text{ff}}. \end{aligned} \tag{9}$$

The feedback controller $K \in \mathcal{R}$ is a form of proportional-integral (PI) structure. Subsequently, Eq (9) becomes as follows:

$$\delta = -\frac{s}{K_{\text{p}}s + K_{\text{i}}}\theta_{\text{ff}}, \tag{10}$$

where the proportional and integral gains $K_{\text{p}} \in \mathbb{R}$ and $K_{\text{i}} \in \mathbb{R}$ are unknown in the retrofit design. As discussed in Section 2, the feed-forward pitch angle θ_{ff} can be calculated based on a steady-state look-up table $\theta_{\text{ff}} = \theta_{\text{ss}}(v_0(t+T))$ and the wind speed v_0 can be computed by filtering and time-delaying the LiDAR measurement $v_{0,L}$. Finally, Eq (10) can be further simplified by a low-pass filter with an adjustable gain $\beta \in \mathbb{R}$ and differentiating the feed-forward pitch angle, expressed as follows:

$$\delta = -\beta\frac{1}{\tau_1 s + 1}\dot{\theta}_{\text{ff}}. \tag{11}$$

3.2. Method 2: modifying the rotor speed measurement with current pitch angle measurement

The retrofit controller modifies the rotor speed measurement with additional knowledge of the current actuator pitch angle. In conventional LiDAR-assisted control, a steady-state feed-forward pitch compensation based on a wind speed look-up table with a time shift is typically implemented. In this method, the retrofit signal with the measurement of pitch angle can make the pitch actuator easier to mimic the feed-forward pitch compensation as used in conventional LiDAR-assisted control. The downside is that this method requires measurement of the angle of the pitch actuator Θ, which complicates the implementation.

Since Method 2 has the actuator pitch angle measurement, the retrofit signal from Eq (11) can be further simplified by substituting the feed-forward pitch rate in Eq (6). This can obviate the need for tuning of the low-pass filter. The retrofit signal becomes as follows:

$$\delta(t) = -\beta\dot{\theta}_{\text{ff}}(t) = -\beta\frac{\theta_{\text{ss}}\left(v_0(t+T)\right) - \theta(t)}{T}. \tag{12}$$

With the retrofit modification, the control objective of the feedback PI controller is slightly changed. The original objective is to regulate the rotor speed, whereas by adding Eq (12) into the rotor speed measurement, the PI controller also minimises the difference between the target steady-state pitch $\theta_{\rm ss}\left(v_0(t+T)\right)$ and current pitch angle $\theta_{\rm a}(t)$. Then, the error fed into the feedback controller is as follows:

$$e(t) = (\Omega_r - \Omega(t)) + \frac{\beta}{T}\left(\theta_{\rm ss}\left(v_0(t+T)\right) - \theta_{\rm a}(t)\right), \tag{13}$$

where the gain β is a design choice to balance between rotor speed regulation and feed-forward pitch matching.

3.3. Method 3: modifying the pitch angle demand and rotor speed measurement

In this approach, the retrofit controller modifies not only the rotor speed measurement, but also the pitch angle reference by adding a pitch signal to the pitch actuator. This approach is similar to conventional LiDAR-assisted control in Eq (6). The main differences to the conventional approaches are that (i) the feed-forward pitch signal is directly added to the pitch actuator instead of the integrator of the feedback; and (ii) re-optimising the feedback gains of the existing controller is achieved by changing the rotor speed measurement. Notice that the hardware implementation of this method is more complicated than the previous two solutions. Some turbine designs might require a full controller retrofit.

The feed-forward pitch demand is an integral of the pitch rate based on Eq (6), defined as follows:

$$\theta_{\rm ff}(t) = \int_0^t \frac{\theta_{\rm ss}\left(v_0(\tau+T)\right) - \theta_{\rm a}(\tau)}{T} d\tau. \tag{14}$$

To re-optimise the feedback controller, the retrofit signal is used as follows:

$$\delta = \alpha(\Omega_r - \Omega), \tag{15}$$

and the feedback pitch demand becomes as follows:

$$\theta_{\rm fb}(t) = \underbrace{K_{\rm p}(1-\alpha)}_{K_{\rm p,new}}(\Omega_r - \Omega(t)) + \underbrace{K_{\rm i}(1-\alpha)}_{K_{\rm i,new}}\int_0^t (\Omega_r - \Omega(\tau))d\tau, \tag{16}$$

where $\alpha \in [0, 1]$ is the gain to reduce the proportional and integral gain in the feedback controller. Notice that the method of re-optimising feedback gain can also be applied to Method 1 and 2.

Typically, in LiDAR-assisted feed-forward control (e.g. [19]), gain reduction in $K_{\rm i}$ should be square of the reduction in $K_{\rm p}$. However, this is not feasible in the retrofit setting since the existing feedback controller remains untouched.

4. Simulation results

This section demonstrates the performance of the proposed LiDAR-assisted retrofit controller by performing simulations.

4.1. Simulation environment and set-up

The turbine model used in this study is a generic 2.3MW wind turbine with a rotor diameter of 92.6 m, and the aeroelastic code is HAWC2 [20] with the Mann turbulence model. The controller employed in this study is the open-source DTU basic controller [21]. The wind speed measurements are from a cost-effective LiDAR[2] with four fixed beams with a focus distance of 100 m. The fatigue load is evaluated using Class 1B wind conditions with annual mean wind speed of 10 m/s [22].

[2] The design is based on WindVision LiDAR manufactured by Windar Photonics.

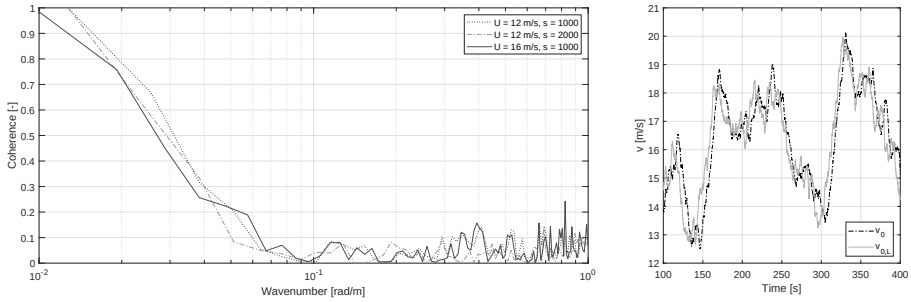

Figure 3: Left: Magnitude-square coherence between the rotor effective wind speed and LiDAR measurements for different wind speeds U and seed numbers s. Right: An example of the time-series of rotor effective wind speed v_0 and LiDAR measurement $v_{0,L}$.

4.2. Measurement coherence

The magnitude-squared coherence is crucial for evaluating the correlation between the LiDAR measurement and the wind speed experienced by the rotor, defined as follows:

$$\gamma^2(k) = \frac{|S_{v_0,v_{0,L}}(k)|^2}{S_{v_0v_0}(k)S_{v_{0,L}v_{0,L}}(k)}, \tag{17}$$

where $S_{v_0,v_{0,L}}$ denotes the cross-power spectral density between the rotor effective wind speed v_0 and the LiDAR measurement $v_{0,L}$, whilst $S_{v_0v_0}, S_{v_{0,L}v_{0,L}}$ are the power spectral densities of v_0 and $v_{0,L}$, respectively. The wave number k at which the magnitude-squared coherence γ^2 drops below 0.5 is commonly used as performance metric (e.g. [23, 24]). This metric is referred as coherence bandwidth $k_{0.5}$, that determines the cut-off frequency of the filter in Eq (3). Figure 3 shows the coherence of three 10-min time-series with different mean wind speeds and seed numbers. The coherent bandwidth is roughly between 0.26 and 0.32 rad/m. Thus, the lowest value is chosen for the cut-off frequency design in Eq (3).

4.3. Case study and discussions on tunings

To illustrate the effectiveness of the proposed retrofit methods, simulations were carried out with a mean wind speed of 15 m/s. Figure 4 shows an example of the time response of the proposed retrofit methods. A clear load reduction of the tower and blade can be seen around 58 s by all retrofit methods.

Tuning can be divided into two parts: (i) time delay and filter for matching the LiDAR measurement to the rotor effective wind speed, as discussed in Section 2; and (ii) the retrofit methods. For the measurement part, the tuning is similar to the conventional LiDAR-assisted control (e.g. [5]). The time delay T_d in Eq (4) is adaptive as it is a function of the mean wind speed $\bar{U}$. The time delay caused by the filter is approximately equal to the filter time constant $T_\mathrm{filter} = \tau_\mathrm{c}$, which is computed based on the $k_{0.5}$ as discussed in Section 4.2, that is also a function of mean wind speed $\bar{U}$. The time τ is assumed to be 0, which needs to be validated in a field experiment as suggested by [5].

For tuning the retrofit methods, the preview time T is chosen to be the time delay T_d in Eq (4). The feed-forward gain β is roughly $1/K_\mathrm{i}$, and filter time-constant τ_1 is roughly K_p/K_i. However, these values are unknown to the retrofit design. They can be identified by some system identification methods, for example, by perturbing the retrofit signal δ and measuring the rotor speed Ω [25]. In addition, given that the order of magnitude of the feedback parameters $K_\mathrm{p}, K_\mathrm{i}$ is similar for different turbines, simulations showed that the retrofit methods with a wide range of feed-forward gain β and filter time-constant τ_1 could still result in a better performance than

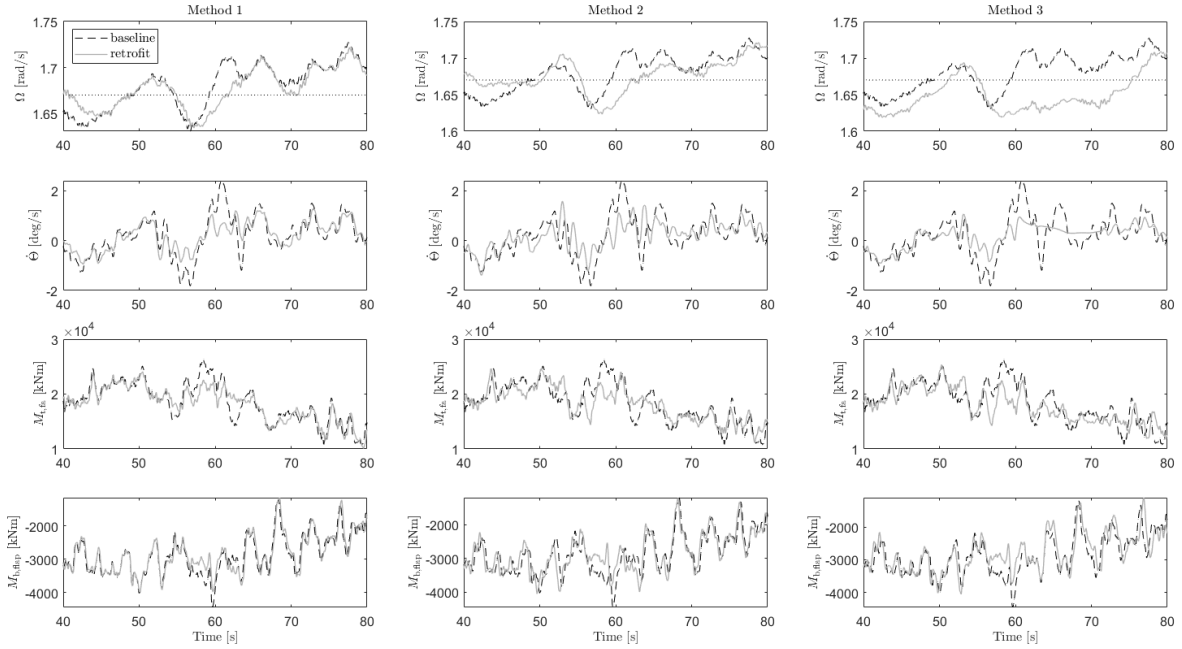

Figure 4: Time-series of rotor speed Ω, pitch rate $\dot{\Theta}$, tower fore-aft moment $M_{\mathrm{t,fa}}$ and blade flap-wise moment $M_{\mathrm{b,flap}}$. Comparison is made between the baseline and each retrofit case. The dotted lines in the rotor speed plots represent the rated rotor speed.

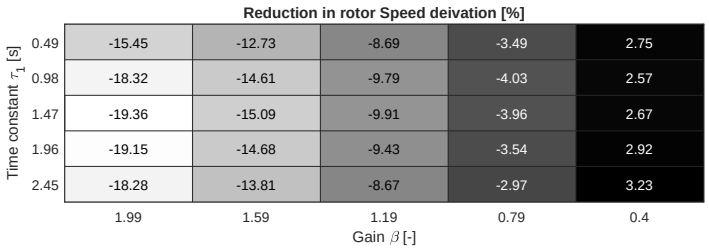

Figure 5: Sensitivity of tuning parameters of Method 1 to the rotor speed deviations. The numbers show the percentage reductions compared to the baseline.

the baseline. Figure 5 shows the sensitivity of tuning parameters of Method 1 to the performance of rotor speed deviations. In this case, the optimal values for τ_1 is 1.47 s and for β is 1.99. It is clear that even the parameters are far from their optimal values, the performance of Method 1 is still better than the baseline. Similarly, the feedback gain reduction α can be tuned to enhance the thrust-related load reductions, discussed in the following section.

4.4. Lifetime fatigue loads

To evaluate the retrofit methods in terms of fatigue load reduction, lifetime damage equivalent loads (DELs) were computed for all proposed methods. Figure 6 shows 20 years lifetime DEL of turbine operating at wind class IB. A clear trend can be seen. The tower fore-aft and side-side lifetime DELs were reduced gradually as the feedback gain is reduced by α, which leads to an increase in the rotor speed deviation. In addition, reducing the feedback gain α could also lower

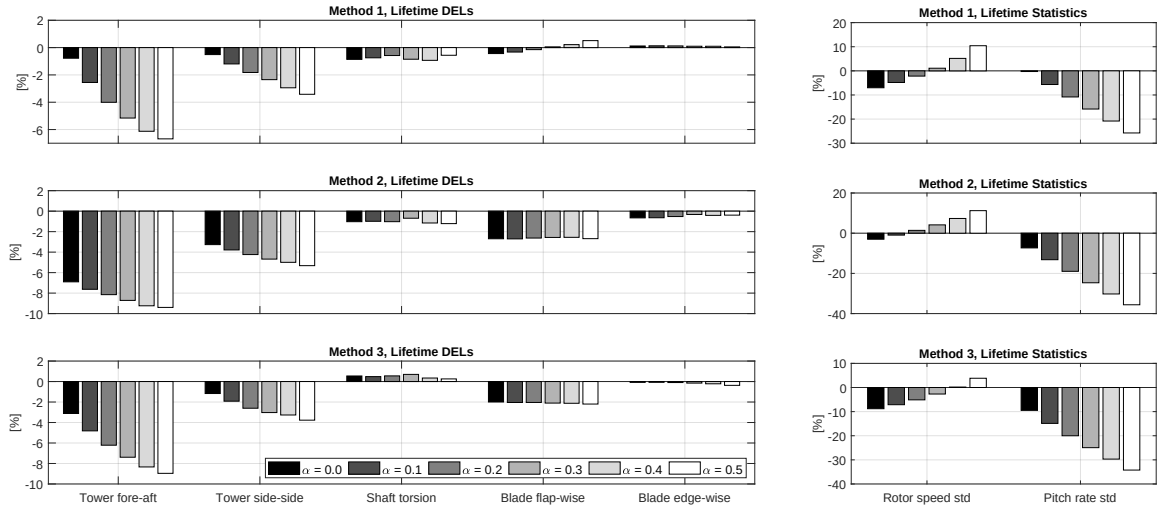

Figure 6: Left: Lifetime fatigue load reduction of tower fore-aft, tower side-side, shaft torsion, blade flap-wise and blade edge-wise. Right: Lifetime statistics of the standard deviation of rotor speed and pitch rate. The greyscale indicates the retrofit controllers with different feedback gain reduction α.

the pitch rate standard deviation, which is reasonable as the high frequency pitch activities were mainly from the feedback controller.

To make a fair comparison in terms of the tower load reductions, some cases were selected where the rotor speed deviation was not deteriorated compared to the baseline (i.e. near 0% reductions). It is clear that the tower load reduction performances between Method 3 (with $\alpha = 0.4$) and Method 2 (with $\alpha = 0.1$) were similar (around 8%), whereas Method 1 (with $\alpha = 0.3$) achieved around 5%. This is expected because of the span in complexity of the retrofit solutions. In Method 2, the current actuator pitch angle in a sense is forced to behave like the feed-forward pitch angle by the feedback controller, whereas, in Method 1, the feed-forward pitch rate is added into the feedback controller without taking into account the current pitch angle of the actuator.

5. Conclusions

The paper demonstrated three LiDAR-assisted retrofit control strategies for enhancing fatigue load reductions. Two of proposed methods (Method 1 and Method 2) provoked the feed-forward pitch angle by modifying the rotor speed measurement. Simulation results were presented that showed all three retrofit method achieved significant load reductions. For example, the lifetime DEL of tower fore-aft moment could be reduced around 5%-8% without deteriorating the rotor speed deviations. Future work will look to investigate the tuning parameters sensitivity of the proposed retrofit methods and validate the proposed methods in a full-scale turbine.

Acknowledgement

This research was supported by the Energy Technology Development and Demonstration Program (EUDP), LiDAR assisted control for reliability improvement (LICOREIM, Grant No. 64019-0580).

References

[1] M. Harris, M. Hand, and A. Wright, "Lidar for Turbine Control," tech. rep., NREL Technical Report, NREL/TP-500-39154, 2005.
[2] D. Schlipf and M. Kuhn, "Prospects of a collective pitch control by means of predictive disturbance compensation assisted by wind speed measurements," in *Proceedings of the 9th German Wind Energy Conference*, 2008.
[3] F. Dunne, D. Schlipf, L. Y. Pao, N. Kelley, A. D. Wright, E. Simley, and B. Jonkman, "Comparison of Two Independent Lidar-Based Pitch Control Designs," in *50th AIAA Aerospace Sciences Meeting Including the New Horzons Forum and Aerospace Exposition*, 2012.
[4] J. Laks, L. Pao, E. Simley, A. Wright, N. Kelley, and B. Jonkman, "Model Predictive Control Using Preview Measurements From LIDAR," in *49th AIAA*, (Reston, Virigina), American Institute of Aeronautics and Astronautics, jan 2011.
[5] D. Schlipf, P. Fleming, F. Haizmann, A. Scholbrock, M. Hofsäß, A. Wright, and P. W. Cheng, "Field Testing of Feedforward Collective Pitch Control on the CART2 Using a Nacelle-Based Lidar Scanner," in *The Science of Making Torque from Wind*, dec 2012.
[6] A. Clifton, P. Clive, J. Gottschall, D. Schlipf, E. Simley, L. Simmons, D. Stein, D. Trabucchi, N. Vasiljevic, and I. Würth, "IEA Wind Task 32: Wind lidar identifying and mitigating barriers to the adoption of wind lidar," *Remote Sensing*, vol. 10, no. 3, 2018.
[7] E. Simley, H. Fürst, F. Haizmann, and D. Schlipf, "Optimizing lidars for wind turbine control applications-Results from the IEA Wind Task 32 workshop," *Remote Sensing*, vol. 10, no. 6, pp. 1–32, 2018.
[8] N. Hure, M. Vašak, M. Jelavić, and N. Perić, "Wind turbine overspeed protection based on polytopic robustly invariant sets," *Wind Energy*, vol. 17, 2015.
[9] V. Petrović and C. L. Bottasso, "Wind turbine envelope protection control over the full wind speed range," *Renewable Energy*, vol. 111, pp. 836–848, 2017.
[10] M. Mirzaei and M. H. Hansen, "A LIDAR-assisted model predictive controller added on a traditional wind turbine controller," in *2016 American Control Conference (ACC)*, pp. 1381–1386, IEEE, jul 2016.
[11] W. H. Lio, B. L. Jones, and J. A. Rossiter, "Preview predictive control layer design based upon known wind turbine blade-pitch controllers," *Wind Energy*, vol. 20, no. 7, pp. 1207–1226, 2017.
[12] W. H. Lio, C. Galinos, and A. M. Urban, "Analysis and design of gain-scheduling blade-pitch controllers for wind turbine down-regulation *," in *2019 IEEE 15th International Conference on Control and Automation (ICCA)*, pp. 708–712, IEEE, jul 2019.
[13] D. Schlipf, D. Trabucchi, O. Bischoff, and M. Hofsäß, "Testing of frozen turbulence hypothesis for wind turbine applications with a scanning LIDAR system," in *Proc. of ISARS*, no. 3, 2010.
[14] D. Schlipf, T. Fischer, and C. Carcangiu, "Load analysis of look-ahead collective pitch control using LIDAR," in *Proc. of 10th German Wind Energy Conference*, 2010.
[15] F. Meng, J. Wenske, and A. Gambier, "Wind turbine loads reduction using feedforward feedback collective pitch control based on the estimated effective wind speed," *Proceedings of the American Control Conference*, vol. 2016-July, pp. 2289–2294, 2016.
[16] E. A. Bossanyi, A. Kumar, and O. Hugues-Salas, "Wind turbine control applications of turbine-mounted LIDAR," *Journal of Physics: Conference Series*, vol. 555, p. 012011, dec 2014.
[17] T. Burton, N. Jenkins, D. Sharpe, and E. Bossanyi, *Wind Energy Handbook*. Chichester, UK: John Wiley Sons, Ltd, may 2011.
[18] H. Canet, S. Loew, and C. L. Bottasso, "What are the benefits of lidar-assisted control in the design of a wind turbine?," *Wind Energy Science*, vol. 6, no. 5, pp. 1325–1340, 2021.
[19] D. Schlipf, E. Bossanyi, C. Carcangiu, and T. Fischer, "LIDAR assisted collective pitch control," *"Integrated Wind Turbine Design"*, no. Deliverable D5.1.3, pp. 1–12, 2011.
[20] T. J. Larsen and A. M. Hansen, "How 2 HAWC2, the user's manual," tech. rep., 2019.
[21] M. H. Hansen and L. C. Henriksen, "Basic DTU Wind Energy controller," Tech. Rep. January, 2013.
[22] IEC, "IEC 61400-1 Ed.3: Wind turbines - Part 1: Design requirements," vol. 2005, 2005.
[23] D. Schlipf, P. W. Cheng, and J. Mann, "Model of the correlation between lidar systems and wind turbines for lidar-assisted control," *Journal of Atmospheric and Oceanic Technology*, vol. 30, no. 10, pp. 2233–2240, 2013.
[24] L. Dong, W. H. Lio, and E. Simley, "On Turbulence Models and LiDAR Measurements for Wind Turbine Control," *Wind Energy Science Discussions*, no. June, pp. 1–16, 2021.
[25] L. Ljung, *System identification: Theory for the user*. Upper Saddle River, NJ, USA: Prentice-Hall, Inc., 1986.